Lightweight Interleaved Residual Dense Network for Gas Identification of Industrial Polypropylene Coupled With an Electronic Nose

Yan Shi, *Member, IEEE*, Hangcheng Yuan, Qinglun Zhang, Ao Sun, Jingjing Liu, and Hong Men

***Abstract*— Polypropylene (PP) is one of the raw materials to produce automotive interior parts. Under the high-temperature condition, the volatile gas of PP will have a pungent odor. Therefore, an effective gas detection method should be proposed. In this work, a lightweight interleaved residual dense network (LIRD) is proposed and coupled with an electronic nose (e-nose) to classify the volatile gas of industrial PP used in the automotive interior. The LIRD combines the lightweight interleaved group convolution (LIGC) and residual dense network (RDN). The LIGC module is proposed to effectively reduce the number of parameters in the convolution calculation and realize the information exchange among channels. To avoid the feature degradation, RDN is introduced to fuse the shallow and deep features, and the parameters are trained adaptively to enhance the classification stability. By means of the self-developed e-nose system, the volatile gas of two PP materials (2240 S and 1120 K) is detected under different temperature gradients. Compared with other deep learning methods, the LIRD has a better classification result of 99.20% and 99.00%, the best F_1-score is 0.9920 and 0.9900, and the best Kappa coefficient is 0.9900 and 0.9875 in two PP materials. The results show that the combination of LIRD and e-nose is demonstrated as an effective analytical technique for quality monitoring in the industrial production process of automotive interior parts.**

***Index Terms*— Electronic nose (e-nose), gas identification, industrial polypropylene (PP), lightweight interleaved residual dense network (LIRD).**

I. Introduction

IN THE industrial production, to reduce manual intervention, it is significant to achieve quality monitoring through the sensor detection technology in combination with the computational intelligence method [1], [2]. Polypropylene (PP) is one of the raw materials for the production of automotive interior parts [3]. Under the high-temperature condition, the volatile gas of PP will produce a pungent odor, which comes from the pure resins, adsorbents, antibacterial agents, light stabilizers, and so on added during the production process [4], [5]. When the PP material is exposed to light, it is easily oxidized and produces various pungent volatile odors, including ketones, aldehydes, and esters [6]. With the high requirement of car manufacturers on the air quality in the car, quality monitoring from raw materials is required. The intensity of volatile gas under different conditions directly reflects the overall quality. Meanwhile, there is a lack of scientific gas measurement instruments and decision-making methods. Quality monitoring mainly relies on manual experience [5], [7], which has the disadvantages of poor repeatability and endangering the health of assessor. Therefore, a fast, accurate, and intelligent detection technology should be proposed.

The electronic nose (e-nose) is an advanced sensor instrument developed based on the principle of human smell perception [8], [9]. It obtains the overall gas information of sample based on the sensor array and makes classification decision by the pattern recognition method [10]. Rehman *et al.* [11] proposed a feature extraction and pattern recognition method that effectively avoids sensor drift compensation. Sarno *et al.* [12] designed an e-nose system and combined it with a support vector machine to detect the pork adulteration in beef. Wang *et al.* [13] used six different gas features combined with a grid search support vector machine to evaluate the trunk borer infestation duration. Zhao *et al*. [14] proposed the weighted discriminative extreme learning machine combined with e-nose to detect the gas of lung cancer patients. Shi *et al.* [8] extracted the time- and time-frequency domain features of detection signal of e-nose and combined them with multiclassifiers to track the quality of rice. In this work, the gas sensor of the metal–oxide–semiconductor (MOS) conductivity type was applied to collect the gas information of PP materials. In previous research, we found that the traditional decision-making process included the feature extraction and pattern recognition, which had two problems.

A. Extracted Features Are Uncertain

For different detection objects, the volatility of gas is different, which will affect the stability of detection signal. If the detection signal is stable, it is suitable to extract features in the time domain [8]. If the detection signal fluctuates greatly, it is suitable to extract features in the time domain and time–frequency domain [13]. If the detection process is complete and the response curve goes through the process of rising, stable, and returning to zero, it is necessary to add the

Manuscript received June 24, 2021; revised September 1, 2021; accepted September 18, 2021. Date of publication October 4, 2021; date of current version October 15, 2021. This work was supported in part by the National Natural Science Foundation of China under Grant 31772059 and Grant 31871882, and in part by the Science and Technology Development Plan of Jilin Province under Grant YDZJ202101ZYTS135. The Associate Editor coordinating the review process was Dr. Wilson Wang. *(Corresponding author: Hong Men.)*

Yan Shi, Hangcheng Yuan, Qinglun Zhang, Jingjing Liu, and Hong Men are with the School of Automation Engineering, Northeast Electric Power University, Jilin 132012, China (e-mail: shiyan@neepu.edu.cn; 2201900390@neepu.edu.cn; 2019303010636@neepu.edu.cn; jingjing_liu@neepu.edu.cn; menhong@neepu.edu.cn).

Ao Sun is with the School of Electrical Engineering, Northeast Electric Power University, Jilin 132012, China (e-mail: 2201900197@neepu.edu.cn).

Digital Object Identifier 10.1109/TIM.2021.3117377

spatial domain features [15]. Meanwhile, different sampling frequencies will also affect the characteristics of detection signal. The time domain, time–frequency domain, and spatial domain contain multiple features selected to represent the overall attributes that will directly affect the final detection accuracy. Therefore, the extracted features are various under different conditions.

B. Verification Process for the Effectiveness of Feature Extraction Is Complicated

After determining the feature extraction method, the effectiveness needs to be verified with the pattern recognition method [12], [13]. If the features have obvious differences, the classifier with the general generalization ability and decision performance can be applied. However, if the differences are small, a classifier with good generalization ability and decision performance is required. Different classifiers also need to select appropriate parameters to improve the decision-making performance. Meanwhile, the feature extraction and classification are two independent processes with low integration. Therefore, the verification process is complicated.

Convolutional neural networks (CNNs) have been widely used in image recognition [16], target detection [17], electroencephalogram (EEG) signal processing [18], fault diagnosis [19], and other fields. It does not need to preprocess the input data, and a well-designed network structure can realize the deep extraction of features [20]. In the CNN training process, the convolution and fully connected (FC) layer parameters are automatically updated by means of the backpropagation method, and the feature extraction and decision process are integrated [21]. The structural design of CNN directly affects the effectiveness of feature extraction. If the number of convolutional layers is fewer, the extracted features may not fully express the overall characteristics of original data. Increasing the number of convolutional layers can obtain the deep features, but the number of parameters will increase, which will lead to feature degradation [22].

However, in the image recognition, target detection, and other fields, a large number of datasets can fully train the parameters, reduce the feature degradation, and enhance the classification performance effectively. E-nose is an advanced sensor instrument developed to avoid the shortcomings of low efficiency and poor reproducibility in the manual detection process. It has the advantages of good reproducibility and high detection efficiency. It is not appropriate to increase the number of samples to improve the classification performance. In the actual industrial inspection process, it is not allowed to obtain many samples. However, the deep network structure increased the number of parameters, which may affect the classification performance. Meanwhile, there is a lack of information interaction among feature channels.

Therefore, the network design of CNN is applied to e-nose information identification should meet:

1) fewer parameters;

2) full interaction of feature information in each channel to improve the effectiveness of feature extraction;

3) avoid the feature degradation.

Based on the design requirements, this article proposes a lightweight interleaved residual dense network (LIRD) for the gas identification of PP materials at different temperatures. The main contributions are as follows.

1) An e-nose system is designed based on the MOS sensor array for volatile gas detection of two PP materials under different temperature gradients.

2) The lightweight interleaved group convolution (LIGC) module is proposed to reduce the number of convolution parameters and achieve the information exchange among channels.

3) The residual dense network (RDN) is introduced to avoid the feature degradation. It merges the shallow and deep features by the local dense connections, and the network parameters are learned adaptively.

In this work, the LIRD combines the LIGC and RDN to intelligently identify the volatile gas of two PP materials used in the automotive interior. It provides a new technology for quality supervision of the industrial manufacturing process. The structure of this work is as follows. Section II describes the related work. Section III shows the method. Section IV shows the experiment and discussion. Finally, Section V draws the conclusion.

II. Related Work

A. Lightweight Network

Without reducing the classification performance, the lightweight network can effectively reduce the trainable parameters of the deep learning algorithm. Chakraborty *et al.* [23] proposed a lightweight deep CNN to identify the chest X-ray image of COVID-19, pneumonia, and normal cases. Saini *et al.* [24] proposed an ultralightweight subspace attention module, which used the calculation method of depth separable convolution (DSC) to reduce the number of parameters by more than 90%. Doriguzzi-Corin *et al.* [25] proposed a practical and lightweight deep learning to classify traffic flows (malicious or benign). Compared with the most advanced data processing technology, this method reduced the calculation time by 40 times. Cui *et al.* [26] designed a lightweight attention module to reduce the calculation difficulty and improve the classification performance on the classification and segmentation of 3-D point clouds. Lv *et al.* [27] proposed a lightweight deep interleaved fusion group convolutional network to reduce parameter redundancy and improve image recognition accuracy. Li *et al.* [28] proposed an interleaved low-rank group convolution hybrid deep network to reduce the number of parameters for identifying the asphalt pavement cracks. Borra *et al.* [29] designed an interpretable and lightweight CNN to analyze the encoding mechanism of EEG. Chen *et al.* [30] proposed a lightweight network with bidirectional constraints to improve the computational efficiency for single image super-resolution.

In previous studies, lightweight network has been widely used in different research fields. It can effectively reduce the number of convolution parameters and improve calculation efficiency and provided feasibility in the network design of e-nose gas recognition.

B. Residual Dense Network

RDN integrates the deep and shallow features through the connection of dense residual blocks and adaptively learns deep and shallow features during the training process, which can effectively avoid feature degradation. Zeineldin *et al.* [31] used a residual neural network and dense convolutional network to construct the U-Net architecture to detect brain tumor lesions. Zhou *et al.* [32] proposed a restructured RDN to improve the flow of features for identifying the different crop disease images. Kokkalla *et al.* [33] proposed a deep dense inception residual network (ResN), which effectively enhanced features' utilization and classification performance on a brain tumor image dataset. Zhang *et al.* [34] proposed an improved RDN to enhance feature fusion and learning ability to recognize optical characters. Adegun and Viriri [35] proposed a new fully convolutional network-based densenet framework composed of connected dense blocks to diagnose skin lesions. Aldoj *et al.* [36] combined the RDN and U-Net to divide the prostate and the prostate zones. Zhai *et al.* [37] proposed an improved single-shot multibox detector method, introducing a dense neural network to fuse deep and shallow features and combined residual blocks to improve the network performance to achieve target detection.

In previous studies, the RDN has proved that it effectively integrates shallow and deep features, improves features' learning ability, and strengthens the model's classification performance. However, it contains many convolution parameters, which increases the difficulty of training the model to a certain extent. The detection data of e-nose have the characteristics of less data. Therefore, this article combines the lightweight network and RDN to realize the gas identification of industrial PP under different temperature gradients.

C. Deep Learning in e-Nose Data Processing

Based on the deep learning method in the application of e-nose gas recognition, Mo *et al.* [38] designed a lightweight network based on the DSC to reduce parameters and improve the detection performance. Gamboa *et al.* [39] used three different structures of CNN to achieve intelligent identification of detected gas. Yoo *et al.* [21] proposed a denoising autoencoder combined with CNN to achieve a good gas recognition result. Cao *et al.* [20] proposed an improved cellular neural network for feature extraction and pattern recognition in gas identification. Zhang *et al.* [40] proposed a channel attention CNN to identify the gas information of liquor. Zhao *et al.* [41] used a 1-D deep CNN to identify the mixture gases. Wang *et al.* [42] used an optimized deep CNN to extract the deep features of gas sensors and identify the gas information of dendrobium.

At present, there are few applications of deep learning in e-nose gas recognition. These methods mainly have the disadvantages of a large number of parameters or low classification stability. After analyzing the characteristics of the e-nose data, we emphasized the design requirements of CNN applied to e-nose gas recognition in the introduction. Next, we will explain the design process of LIRD, use the self-developed e-nose to obtain the gas information of industrial PP, and combine the comparison results of multiple models to verify the effectiveness of LIRD.

III. METHOD

It has been explained that the design requirements of CNN should have a small number of parameters and the feature information of each channel should be fully interacted with the feature degradation avoided. Therefore, this article proposes the LIRD, which combines the LIGC and RDN modules. The LIGC module is designed to reduce the number of parameters and realize the feature interaction among channels, and then, the RDN module is introduced to avoid feature degradation. In the traditional convolution calculation process, without setting the convolution bias, the parameter calculation formula of CNN can be expressed as

$$\text{Params} = S \cdot L \cdot M \tag{1}$$

where S represents the size of convolution kernel, L is the number of input channels, and M denotes the number of output channels.

A. Depth Separable Convolution

DSC includes channel convolution and point convolution. Channel convolution splits the multichannel feature matrix into a single-channel feature matrix, performs single-channel convolution, and then merges them. The point convolution uses a convolution kernel of 1×1 for calculation. In the calculation process of DSC, channel convolution is used for calculation first, and then, point convolution is implemented. Without reducing the classification performance, the lightweight calculation process can reduce the number of parameters in traditional convolution calculations [25]. The parameter calculation formula of DSC can be expressed as

$$\text{Params}_{\text{DSC}} = S \cdot L + L \cdot M. \tag{2}$$

B. Lightweight Interleaved Group Convolution

The interleaved group convolution (IGC) can reduce the number of parameters of convolution process without reducing the classification performance and effectively realize the information exchange among channels, which includes two group convolutions [43]. Primary group convolution groups the input channels and then convolves each group separately. It can lighten the convolution process and increase the calculation speed. However, information exchange cannot be achieved among grouped convolutions, and the convolution process cannot achieve information complementarity. Therefore, the second group convolution is proposed to achieve the information complementarily, and the input channels of each group come from different groups in the primary group convolution. When the point convolution performs channel fusion, the information interaction can be realized while reducing the amount of calculation. The parameter calculation formula of IGC can be expressed as follows:

$$\text{Params}_{\text{IGC}} = S \cdot Q \cdot G \cdot G + G \cdot Q \cdot Q \tag{3}$$

where Q represents the number of input channels divided into groups and G represents the number of channels contained in each group. The size of feature matrix remains unchanged in the IGC.

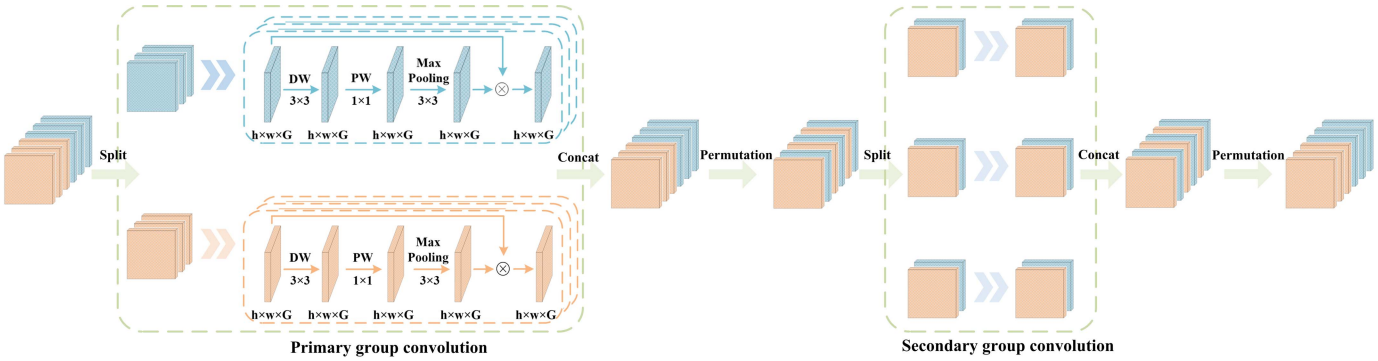

Fig. 1. Illustrating the LIGC.

However, although the parameter reduction is realized in the primary group convolution, the convolution form is still the traditional calculation process. The DSC is introduced to further compress the number of convolution parameters and enhance the calculation speed, and the maximum pooling operation is added to realize the spatial domain attention. The output result of the maximum pooling is multiplied by the input, and the feature attention is realized. In the grouped convolution process, the calculation formula of module can be expressed as follows:

$$\text{Out} = \text{maxpool}^{3\times3,1}\left(\text{PW}^{1}\left(\text{DW}^{3\times3,1}(\text{In})\right)\right) \otimes \text{In} \tag{4}$$

where $\text{maxpool}^{3\times3,1}$ denotes the maximum pooling with the pooling size 3×3 and padding 1, $\text{DW}^{3\times3,1}$ represents the depthwise convolution with kernel size 3×3 and padding 1, PW^{1} represents the pointwise convolution, In is the input of subspace, Out is the output of subspace, and $\otimes$ is the elementwise multiplication. The number of parameters in the subspace module comes from the DSC. The parameter calculation formula of subspace module can be expressed as follows:

$$\text{Params}_{\text{subspace module}} = 9 \cdot G + G \cdot G. \tag{5}$$

Therefore, we combine the IGC and DSC with an attention mechanism to form an LIGC module to compress convolution parameters and realize the information exchange among channels. The parameter calculation formula of LIGC can be expressed as follows:

$$\text{Params}_{\text{LIGC}} = Q \cdot (9 \cdot G + G \cdot G) + G \cdot Q \cdot Q. \tag{6}$$

To visualize the calculation process of LIGC, the input is six channels, divided into two groups, and each group has three channels as an example. Fig. 1 shows the module structure of LIGC and the IGC is the mainframe, replacing the convolution calculation of primary group convolution with the subspace module, where $h \times w$ represents the size of feature matrix of input.

C. Lightweight Interleaved Residual Dense Network

In the calculation process of CNN, the effectiveness of extracted features can be enhanced by deepening the number of convolution layers. Therefore, when constructing a CNN, the deeper the network is, the richer the features can be extracted, whereas deeper features may cause feature degradation, that is, as the number of network layers increases, effective features may be destroyed. Therefore, we introduce an RDN module, which combines the shallow and deep features using local dense connections and adaptively learns the features of each convolutional layer by network training [44].

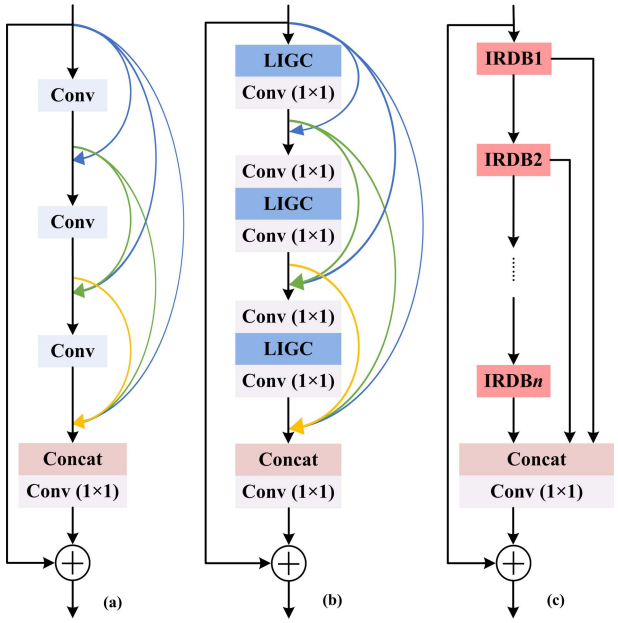

Fig. 2. Illustrating the LIRD: (a) RDB, (b) IRDB, and (c) LIRD.

RDN is composed of several residual dense blocks (RDBs). Fig. 2(a) shows the structure of traditional RDB, which includes three residual dense connections. In this way, the shallow and deep features are connected adaptively within the dense block, and then, the three-layer features are connected. The point convolution operation is used to adjust the number of channels, and then, the input features are fused.

However, in the calculation process of RDB, the convolution block is still a traditional calculation process. It does not reduce the number of parameters, the information among channels is not sufficiently interacted, and the key features are not paid attention. Therefore, based on the LIGC module, the convolution block in RDB is replaced. Fig. 2(b) shows the improved RDB (IRDB), where the LIGC module replaces the

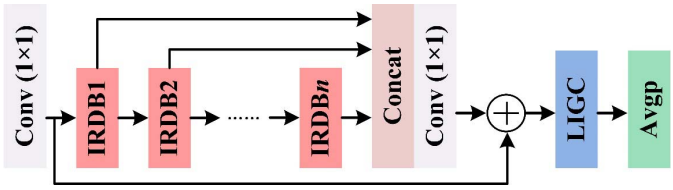

Fig. 3. Network structure for gas identification of PP.

convolution calculation in the RDB. In the IRDB, the point convolution after LIGC is to realize the information compression, and the point convolution calculation before LIGC is to realize the channel adjustment for the calculation of LIGC.

Therefore, the combination of LIGC and RDB can effectively reduce the number of parameters, realize the information exchange among feature channels, and adaptively connect the shallow and deep features to avoid the feature degradation effectively. Based on the IRDB in Fig. 2(b), Fig. 2(c) shows the LIRD. The dense connection form within the dense block is maintained, and the residual connection among the IRDBs is applied. Through the network training, the deep and shallow features are adaptively learned. In the LIRD, the number of IRDB is determined in Section IV.

D. Network Structure for Gas Identification

Fig. 3 shows the network structure, which is applied to the gas identification of two PP materials. First, the point convolution calculates the original detection information to expand the single channel to multiple channels for the feature depth extraction. Second, the LIRD is used to extract the depth features. It is composed of several IRDB modules, and the structure of IRDB is shown in Fig. 2(b). In this way, not only the number of parameters is reduced, but also the information interaction among channels is enhanced. The deep and shallow features are merged, effectively avoiding feature degradation. Third, the LIGC module is used to perform the calculation on the output of LIRD. Finally, the average pooling is applied to compress the features output and then input features to the FC layer for the classification decision.

IV. Experiment and Discussion

The developed LIRD was implemented in Pytorch 1.8.1. Data were processed on a computer with an i5-8400 central processing unit.

A. Samples

Two different types of PP particles were provided by PetroChina Ningxia Petrochemical Company, Yinchuan, China. One is the high-strength PP with model 2240 S. The other is the high-heat-resistant PP particles with model 1102 K. The materials were used for automotive interior parts, stored in a low-temperature and dry environment before the experiment. When it is exposed to light, the PP material is easily oxidized under the high-temperature condition, producing a pungent odor. We tested the volatile gas of PP materials at different temperatures under laboratory conditions and explored the feasibility of quality detection based on the e-nose technology. Two PP materials were heated under different temperature gradients (30 °C, 40 °C, 50 °C, 60 °C, and 70 °C), based on the gas sensor array to detect the volatile gas.

TABLE I
Main Parameters of Ten MOS Sensors

No.	Sensors	Sensitivity	Detection range (ppm)
1	MQ-2	Combustible gas, smoke	300-10000
2	MQ-135	Ammonia, sulfide	10-1000
3	TGS-825	Hydrogen sulfide	5-100
4	WSP-2110	Formaldehyde, benzene, alcohol	1-50
5	MP-503	Alcohol, isobutane, formaldehyde	1-1000
6	TGS-2602	Toluene, organic solvent	1-30
7	WSP-1110	Nitrogen Dioxide	0.1-10
8	MQ-138	Toluene, acetone, ethanol	5-500
9	MQ-137	Ammonia	5-500
10	MQ-136	Hydrogen sulfide	1-200

B. E-Nose

Fig. 4 shows the structure of the self-developed e-nose system. By means of the cross-sensitive sensor array, the self-developed e-nose obtains the comprehensive gas information of PP materials. The gas circuit system includes a gas chamber unit, a flow measurement sensor, and several solenoid valves. In the layout, the length of gas path should be shortened without affecting the working characteristics of detection elements. The sensor air chamber is composed of a cover plate, a printed circuit board (PCB) board, a sealing plate, a sensor array, and a cavity. The outer shape of air chamber is designed as a rectangle for easy installation, the inner cavity is designed as a cylinder shape, and the main body is 304 stainless steel. The surface of PCB is wrapped with polytetrafluoroethylene nonadsorbing material, which reduces the surface temperature and effectively prevents damage to the mounting plate caused by long-term heating of sensors. The sensor array is composed of ten MOS gas sensors. Table I shows the names, sensitivity, and detection range of gas sensors. The constant temperature heating device includes a heating module and a heating plate, and it can realize constant temperature heating of sample during the sampling process. The heating plate is made of aluminum alloy material with high thermal conductivity. The metal bath heating method can improve the heat transfer efficiency of sample and reduce energy consumption. The air pressure and clean air are provided by an air generator, which includes a high-efficiency four-stage purification device, an air tank, and an air pipeline. It can effectively avoid baseline drift. Among them, the high-efficiency four-stage purification device can effectively filter moisture and extend the service life of filter.

In the test, the response value can be obtained, namely R_0/R_S. R_0 represents the sensor's conductivity in contact with the sample gas and R_S denotes the sensor's conductivity in contact with the clean gas filtered by the air generator. When the tested gas is in contact with the sensor, an oxidation–reduction reaction will occur, changing the conductivity of

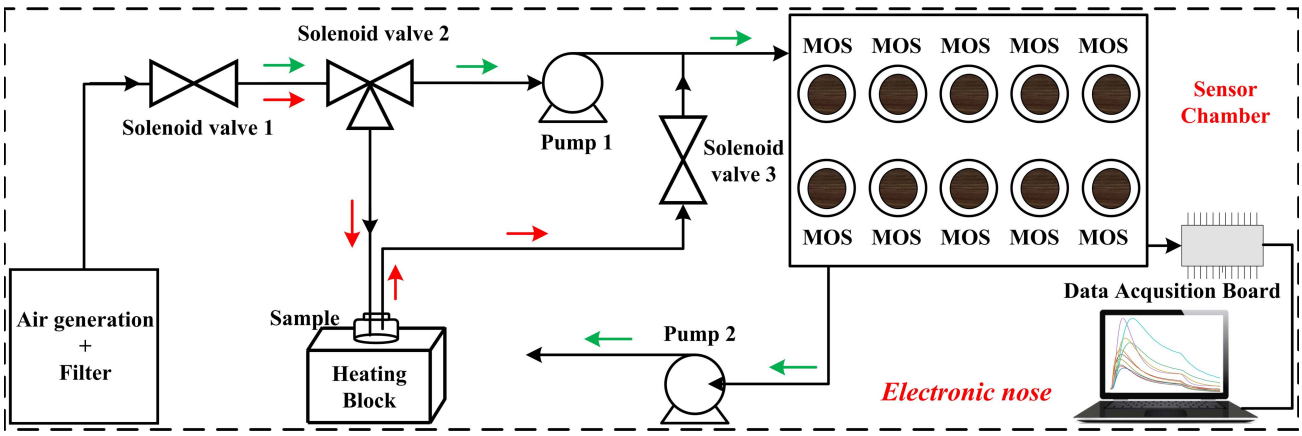

Fig. 4. Structure of the self-developed e-nose system.

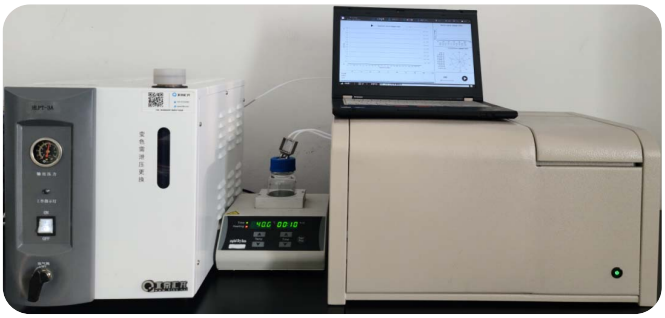

Fig. 5. Appearance of e-nose system.

the sensor's active material and finally achieving the volatile gas detection. The EM9636M data acquisition card (Beijing Zhongtai Lianchuang Technology Company Ltd., Beijing, China) is used to convert gas information into digital signals and transmit them to a computer for storage and processing. Fig. 5 shows the appearance of e-nose system.

C. Experiment

In the experiment, the environment temperature was 23 °C ± 0.5 °C. The volatile gas detection of 2240 S and 1120 K materials had the same experimental procedure. After the preexperiment, the experimental steps were as follows.

1) The e-nose was turned on for 1 h. Preheat the gas sensor to ensure stable output. The air storage tank of air generator was pressed, and the high-pressure air was injected into the gas circuit. The pressure change of each section in the gas circuit was monitored to confirm no leakage fault in the system.
2) Cleaning of the gas circuit and gas chamber. The high-pressure air in the air generator was used to clean the sample bottle, the entire gas circuit, and the air chamber to eliminate the influence of gas residue on the experiment. The cleaning time was 180 s.
3) Gas information detection of PP materials; 20 g of PP particles were put into a 200-mL sample bottle, and the sample bottle was placed in the heating module and heated for 10 min. After the headspace in the bottle volatilized sufficiently, the gas information collection started, where the sampling frequency of sensors was 1 Hz and the flow rate was 600 mL/min. The sampling time of sensors was 100 s, which consisted of 60 s for detecting the sample gas, and 40 s was filled with clean air.
4) Repeat steps 2 and 3 for repetitive experiments. Without loss of generality, the number of parallel samples was 40 for each temperature gradient, and a total of 200 samples were obtained. Fig. 6 shows the response curve of 2240 S material under different temperature gradients.

D. Hyperparameter Setup

The detection data of PP material obtained 40 parallel samples at each temperature, from which 30 groups were randomly selected as the training set to build the classification model, and the remaining ten groups were used as the testing set to test the classification performance. Therefore, each PP material contained a total of 150 training sets and 50 testing sets. To eliminate the randomness, the classification accuracy, F_1-score, and Kappa coefficient were the average of ten calculations.

The optimization-related hyperparameters were preadjusted in the training process. The FC layer of LIRD contained five neurons, which was consistent with the number of categories. The number of FC was 1. In the model's training process, the batch size was 20, and the number of iterations was 100. The Adam optimizer with a 0.01 learning rate was selected to update the parameters. After each module performed the convolution calculation, the batch normalization was used to maintain the same data distribution and speed up training [22], and the activation function of rectified linear unit (ReLU) was used. In the loss function, the L2 penalty term was introduced to reduce the overfitting phenomenon, and the loss function equation was as follows:

$$\text{loss} = -\sum_{i=1}^{5} y_i \log(\hat{y}_i) + \lambda \left\| \sum_{j=1}^{n} \omega_j^2 + b_j^2 \right\| \tag{7}$$

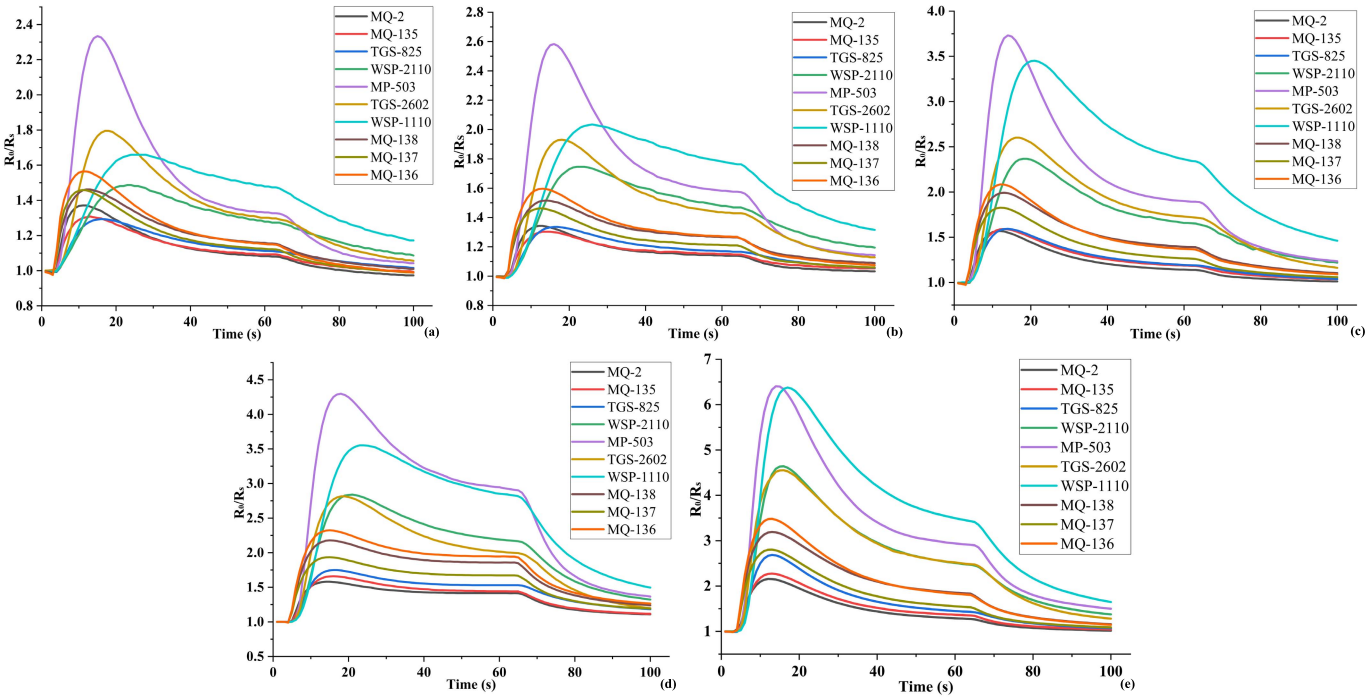

Fig. 6. Response curve of 2240 S material under different temperatures: (a) 30 °C, (b) 40 °C, (c) 50 °C, (d) 60 °C, and (e) 70 °C.

TABLE II
PARAMETERS OF ONE IRDB

Operation	Group	Input size	Output size
LIGC	4×3	100×10×12	100×10×12
Conv	1	100×10×12	100×10×1
Conv	1	100×10×13	100×10×12
LIGC	6×2	100×10×12	100×10×12
Conv	1	100×10×12	100×10×1
Conv	1	100×10×14	100×10×12
LIGC	4×3	100×10×12	100×10×12
Conv	1	100×10×12	100×10×1
Conv	1	100×10×15	100×10×12

where $\lambda = 0.01$, y_i is the actual category, $\hat{y}_i$ denotes the predicted category, and ω_j and b_j are the weights and thresholds of FC, respectively.

In Section I, we emphasized the design conditions of CNN applied to e-nose information recognition. Since the detection data of e-nose is small, in the convolution calculation process, if the number of feature channels is too large, it will increase the number of parameters and the difficulty of gas recognition. Meanwhile, too few feature channels may cause insufficient in the feature extraction. Therefore, to extract the detection features of e-nose, the convolution parameters were preadjusted. We used the point convolution to expand the original data into the feature matrix of 12 channels, and the LIRD was applied for feature mining. In the LIRD, it was composed of several IRDB modules. Table II shows the parameters for one IRDB module.

After the calculation of LIRD, the LIGC module with 6 × 2 groups was used to calculate the output, and then, the average pooling (Avgp) with 2 × 1 kernel size was applied to compress the feature output. In the LIRD, the number of IRDB modules directly affected the number of parameters and decision accuracy. Table III shows the gas identification results of two PP materials with a different number of IRDB modules. The results were the average ± standard deviation of ten calculations. When the LIRD was composed of one IRDB module, the classification accuracy of 2240 S was 99.20% in the testing set, and the 1102 K was 99.00%. With the number of IRDB increased, the network's overall performance was not improved and slightly decreased, the model parameters were increased, and the classification stability fluctuated. Therefore, the LIRD, including one IRDB module, was determined. Fig. 7 shows the final structure of LIRD, which was applied to the gas recognition of PP.

TABLE III
INFLUENCE OF THE NUMBER OF IRDB ON THE CLASSIFICATION PERFORMANCE OF LIRD

No.	Structure	Testing accuracy (%) 2240 S	1102 K
1	Conv-IRDB-LIGC-Avgp	99.20±1.03	99.00±1.05
2	Conv-IRDB×2-LIGC-Avgp	99.00±1.41	99.00±1.70
3	Conv-IRDB×3-LIGC-Avgp	98.20±2.00	99.00±1.40
4	Conv-IRDB×4-LIGC-Avgp	98.80±1.40	98.60±1.65

E. Comparison of Decision Results (Multimodels)

To illustrate the effectiveness of LIRD, we compared it with other architecture-related networks. Table IV shows the network structures and convolution parameters of comparison models, including the CNN, DSC, IGC, LIGC, ResN,

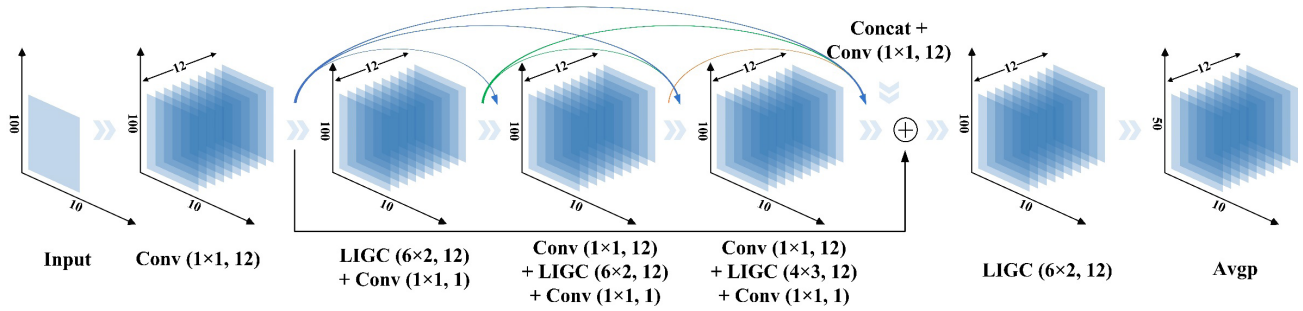

Fig. 7. Final network structure for gas identification of PP.

TABLE IV
NETWORK STRUCTURES AND CONVOLUTION PARAMETERS OF COMPARISON MODELS

Step	CNN	DSC	IGC	LIGC	ResN	RDN
1	Input	Input	Input	Input	Input	Input
2	Conv(1×1, 12, 0)	Conv(1×1, 12, 0)	Conv(1×1, 12, 0)	Conv(1×1, 12, 0)	Conv(1×1, 12, 0)	Conv(1×1, 12, 0)
3	Conv(3×3, 12, 1)	DSC(3×3, 12, 1)	IGC(4, 3, 12)	LIGC(4, 3, 12)	Conv(3×3, 12, 1)	Conv(3×3, 1, 1)
4	Conv(3×3, 12, 1)	DSC(3×3, 12, 1)	IGC(6, 2, 12)	LIGC(6, 2, 12)	Conv(3×3, 12, 1)	Conv(3×3, 1, 1)
5	Conv(3×3, 12, 1)	DSC(3×3, 12, 1)	IGC(4, 3, 12)	LIGC(4, 3, 12)	Conv(3×3, 12, 1)	Conv(3×3, 1, 1)
6	Conv(3×3, 12, 1)	DSC(3×3, 12, 1)	IGC(6, 2, 12)	LIGC(6, 2, 12)	Conv(3×3, 12, 1)	Conv(3×3, 12, 1)
7	Avgp(2×1, 12, 0)	Avgp(2×1, 12, 0)	Avgp(2×1, 12, 0)	Avgp(2×1, 12, 0)	Avgp(2×1, 12, 0)	Avgp(2×1, 12, 0)

TABLE V
CLASSIFICATION RESULTS OF MULTINETWORK

Model	#Params	2240 S			1102 K		
		Accuracy (%)	F_1-score	Kappa	Accuracy (%)	F_1-score	Kappa
CNN	5196	96.00±3.12	0.9624±0.03	0.9525±0.04	96.20±3.94	0.9585±0.04	0.9475±0.05
DSC	1020	96.70±2.37	0.9645±0.03	0.9545±0.03	96.80±3.05	0.9676±0.03	0.9560±0.04
IGC	1332	97.20±1.70	0.9723±0.02	0.9650±0.02	96.80±2.70	0.9682±0.03	0.9600±0.03
LIGC	804	97.60±1.42	0.9742±0.01	0.9685±0.02	97.80±1.98	0.9720±0.02	0.9650±0.03
ResN	5196	96.60±2.82	0.9647±0.03	0.9560±0.03	96.20±2.88	0.9605±0.03	0.9550±0.04
RDN	1839	96.60±1.65	0.9644±0.02	0.9550±0.03	97.60±1.84	0.9761±0.02	0.9700±0.02
LIRD	1344	99.20±1.03	0.9920±0.01	0.9900±0.01	99.00±1.05	0.9900±0.01	0.9875±0.01

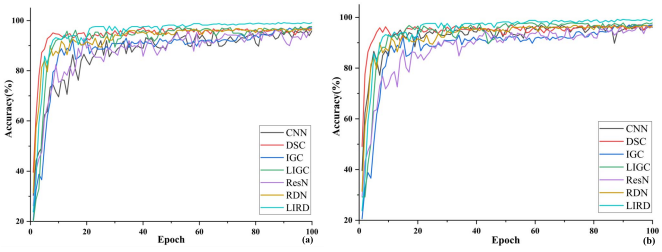

Fig. 8. Accuracy change curve in testing set: (a) 2240 S and (b) 1102 K.

and RDN. In the Conv and DSC ($n \times n$, m, and 0/1), $n \times n$ denotes the convolution kernel size, m represents the number of output channels, 0 means adding padding, and 1 means no adding padding.

In the IGC and LIGC, the first number represented the number of groups, the second number was the number of channels in each group, and the third number denoted the total number of channels. In the ResN, steps 3–5 were used as residual blocks. The average pooling process was the same as the LIRD.

The parameters of FC in each model were consistent with the LIRD. Fig. 8 shows each model's classification accuracy change curve for two PP materials in the testing set. In the overall change of curve, the overall classification stability of CNN and ResN was poor. The LIRD had not only the best classification accuracy but also the best classification stability.

Table V shows the performance comparison results of classification accuracy, F_1-score, and Kappa coefficient of two PP materials in the testing sets. The comparison results were the average ± standard deviation of ten calculations. The number of parameters in the traditional convolution calculation process was 5196, the DSC reduced by 80.37%, the IGC reduced by 74.36%, the LIGC reduced by 84.53%, the RDN reduced by 64.61%, and the LIRD reduced by 74.13%. In the classification results of 2240 S PP material, the IGC improved the classification performance to a certain extent. The LIGC reduced the parameters significantly and improved the classification accuracy by 1.6%. The classification performance of LIGC was better than that of the CNN, DSC, IGC, and ResN. It was not obvious that the RDN improved the classification performance, but the classification stability was improved. Compared with other models, the LIRD had the best classification performance. The classification accuracy was 99.20%, the F_1-score was 0.9920, the Kappa coefficient was 0.9920, and the structure had the best classification stability. In the

classification results of 1102 K PP material, the classification accuracy of ResN was unchanged, and classification stability was improved. The DSC, IGC, LIGC, and RDN improved the classification performance to a certain extent, and the RDN enhanced the classification stability obviously. Meanwhile, compared with other models, the LIRD still obtained the best classification performance. The classification accuracy was 99.00%, the F_1-score was 0.9900, and the Kappa coefficient was 0.9875. The model had the best classification stability.

V. Conclusion

In this work, to classify the volatile gas of two PP materials under different temperature gradients, an LIRD is proposed to automatically extract and classify the depth features of original data of e-nose. The main conclusions are as follows.

1) An e-nose is developed based on an MOS sensor array. The instrument is equipped with an air generator and a constant temperature heating device to collect the gas information of PP materials.

2) An LIGC module is proposed to effectively reduce the number of parameters in the convolution process and realize the information exchange among channels. In this process, the number of convolution parameters is reduced to 84.53% effectively, and the IRDB is proposed to avoid the feature degradation.

3) The multimodels comparison results show that the LIRD achieves the best classification performance. Under the 2240 S PP material, the classification accuracy of testing set is 99.20%, the F_1-score is 0.9920, and the Kappa coefficient is 0.9900. Under the 1102 K PP material, the classification accuracy of testing set is 99.00%, the F_1-score is 0.9900, and the Kappa coefficient is 0.9875. Meanwhile, the best classification stability is obtained.

In conclusion, the deep learning method requires no preprocessing of gas information, integrates the feature extraction and classification processes, and realizes the intelligent identification of PP materials gas information. Moreover, it can be used as an effective detection method for quality monitoring in the industrial production process of automotive interior parts.

References

[1] Y. Cheng, K.-Y. Wong, K. Hung, W. Li, Z. Li, and J. Zhang, "Deep nearest class mean model for incremental odor classification," *IEEE Trans. Instrum. Meas.*, vol. 68, no. 4, pp. 952–962, Apr. 2019.

[2] Y. Shi *et al.*, "Improving performance: A collaborative strategy for the multi-data fusion of electronic nose and hyperspectral to track the quality difference of rice," *Sens. Actuators B, Chem.*, vol. 333, Apr. 2021, Art. no. 129546.

[3] A. V. Genis, "Analysis of the global and Russian markets of polypropylene and of its main consumption areas," *Russian J. Gen. Chem.*, vol. 87, no. 9, pp. 2137–2150, Sep. 2017.

[4] Y.-C. Chien, "Variations in amounts and potential sources of volatile organic chemicals in new cars," *Sci. Total Environ.*, vol. 382, nos. 2–3, pp. 228–239, Sep. 2007.

[5] J. Li *et al.*, "Odor assessment of automobile cabin air with field asymmetric ion mobility spectrometry and photoionization detection," *IEEE Sensors J.*, vol. 16, no. 2, pp. 409–417, Jan. 2016.

[6] Q. Xiang, M. Xanthos, S. Mitra, S. H. Patel, and J. Guo, "Effects of melt reprocessing on volatile emissions and structural/rheological changes of unstabilized polypropylene," *Polym. Degradation Stability*, vol. 77, no. 1, pp. 93–102, Jan. 2002.

[7] J. Li *et al.*, "Using field asymmetric ion mobility spectrometry for odor assessment of automobile interior components," *IEEE Sensors J.*, vol. 16, no. 14, pp. 5747–5756, Jul. 2016.

[8] Y. Shi, X. Jia, H. Yuan, S. Jia, J. Liu, and H. Men, "Origin traceability of rice based on an electronic nose coupled with a feature reduction strategy," *Meas. Sci. Technol.*, vol. 32, no. 2, Feb. 2021, Art. no. 025107.

[9] L. Dutta, C. Talukdar, A. Hazarika, and M. Bhuyan, "A novel low-cost hand-held tea flavor estimation system," *IEEE Trans. Ind. Electron.*, vol. 65, no. 6, pp. 4983–4990, Jun. 2018.

[10] Y. Shi, M. Liu, A. Sun, J. Liu, and H. Men, "A fast Pearson graph convolutional network combined with electronic nose to identify the origin of rice," *IEEE Sensors J.*, early access, May 12, 2021, doi: 10.1109/JSEN.2021.3079424.

[11] A. U. Rehman, S. B. Belhaouari, M. Ijaz, A. Bermak, and M. Hamdi, "Multi-classifier tree with transient features for drift compensation in electronic nose," *IEEE Sensors J.*, vol. 21, no. 5, pp. 6564–6574, Mar. 2021.

[12] R. Sarno, K. Triyana, S. I. Sabilla, D. R. Wijaya, D. Sunaryono, and C. Fatichah, "Detecting pork adulteration in beef for halal authentication using an optimized electronic nose system," *IEEE Access*, vol. 8, pp. 221700–221711, 2020.

[13] Z. Wang, W. Chen, S. Gu, Y. Wang, and J. Wang, "Evaluation of trunk borer infestation duration using MOS E-nose combined with different feature extraction methods and GS-SVM," *Comput. Electron. Agricult.*, vol. 170, Mar. 2020, Art. no. 105293.

[14] L. Zhao *et al.*, "A weighted discriminative extreme learning machine design for lung cancer detection by an electronic nose system," *IEEE Trans. Instrum. Meas.*, vol. 70, 2021, Art. no. 2509709.

[15] S. Zhang, C. Xie, M. Hu, H. Lia, Z. Baia, and D. Zeng, "An entire feature extraction method of metal oxide gas sensors," *Sens. Actuators B, Chem.*, vol. 132, no. 1, pp. 81–89, 2008.

[16] C. Hu and Y. Wang, "An efficient convolutional neural network model based on object-level attention mechanism for casting defect detection on radiography images," *IEEE Trans. Ind. Electron.*, vol. 67, no. 12, pp. 10922–10930, Dec. 2020.

[17] N. Kousik, Y. Natarajan, R. Arshath Raja, S. Kallam, R. Patan, and A. H. Gandomi, "Improved salient object detection using hybrid convolution recurrent neural network," *Expert Syst. Appl.*, vol. 166, Mar. 2021, Art. no. 114064.

[18] J. Cao, J. Zhu, W. Hu, and A. Kummert, "Epileptic signal classification with deep EEG features by stacked CNNs," *IEEE Trans. Cognit. Develop. Syst.*, vol. 12, no. 4, pp. 709–722, Dec. 2020.

[19] S. Guo, B. Zhang, T. Yang, D. Lyu, and W. Gao, "Multitask convolutional neural network with information fusion for bearing fault diagnosis and localization," *IEEE Trans. Ind. Electron.*, vol. 67, no. 9, pp. 8005–8015, Sep. 2020.

[20] H. Cao, P. Jia, D. Xu, Y. Jiang, and S. Qiao, "Feature extraction of citrus juice during storage for electronic nose based on cellular neural network," *IEEE Sensors J.*, vol. 20, no. 7, pp. 3803–3812, Apr. 2020.

[21] Y. Yoo, H.-I. Kim, and S.-I. Choi, "Robust classification of largely corrupted electronic nose data using deep neural networks," *IEEE Sensors J.*, vol. 21, no. 4, pp. 5052–5059, Feb. 2021.

[22] M. Zhao, S. Zhong, X. Fu, B. Tang, and M. Pecht, "Deep residual shrinkage networks for fault diagnosis," *IEEE Trans. Ind. Informat.*, vol. 16, no. 7, pp. 4681–4690, Jul. 2020.

[23] M. Chakraborty, S. V. Dhavale, and J. Ingole, "Corona-nidaan: Lightweight deep convolutional neural network for chest X-ray based COVID-19 infection detection," *Int. J. Speech Technol.*, vol. 51, no. 5, pp. 3026–3043, May 2021.

[24] R. Saini, N. K. Jha, B. Das, S. Mittal, and C. K. Mohan, "ULSAM: Ultra-lightweight subspace attention module for compact convolutional neural networks," in *Proc. IEEE Winter Conf. Appl. Comput. Vis. (WACV)*, vol. 1, Mar. 2020, pp. 1616–1625.

[25] R. Doriguzzi-Corin, S. Millar, S. Scott-Hayward, J. Martinez-del-Rincon, and D. Siracusa, "Lucid: A practical, lightweight deep learning solution for DDoS attack detection," *IEEE Trans. Netw. Service Manage.*, vol. 17, no. 2, pp. 876–889, Jun. 2020.

[26] Y. Cui, Y. An, W. Sun, H. Hu, and X. Song, "Lightweight attention module for deep learning on classification and segmentation of 3-D point clouds," *IEEE Trans. Instrum. Meas.*, vol. 70, 2021, Art. no. 2500912.

[27] E. Lv, Y. Cheng, X. Wang, and C. L. P. Chen, "Deep convolutional network based on interleaved fusion group," *IEEE Trans. Cognit. Develop. Syst.*, vol. 13, no. 3, pp. 555–565, Sep. 2021.

[28] G. Li, Q. Liu, W. Ren, W. Qiao, B. Ma, and J. Wan, "Automatic recognition and analysis system of asphalt pavement cracks using interleaved low-rank group convolution hybrid deep network and SegNet fusing dense condition random field," *Measurement*, vol. 170, Jan. 2021, Art. no. 108693.
[29] D. Borra, S. Fantozzi, and E. Magosso, "Interpretable and lightweight convolutional neural network for EEG decoding: Application to movement execution and imagination," *Neural Netw.*, vol. 129, pp. 55–74, Sep. 2020.
[30] L. Chen, L. Guo, D. Cheng, Q. Kou, and R. Gao, "A lightweight network with bidirectional constraints for single image super-resolution," *Optik*, vol. 239, Aug. 2021, Art. no. 166818.
[31] R. A. Zeineldin, M. E. Karar, J. Coburger, C. R. Wirtz, and O. Burgert, "DeepSeg: Deep neural network framework for automatic brain tumor segmentation using magnetic resonance FLAIR images," *Int. J. Comput. Assist. Radiol. Surg.*, vol. 15, no. 6, pp. 909–920, Jun. 2020.
[32] C. Zhou, S. Zhou, J. Xing, and J. Song, "Tomato leaf disease identification by restructured deep residual dense network," *IEEE Access*, vol. 9, pp. 28822–28831, 2021.
[33] S. Kokkalla, J. Kakarla, I. B. Venkateswarlu, and M. Singh, "Three-class brain tumor classification using deep dense inception residual network," *Soft Comput.*, vol. 25, no. 13, pp. 8721–8729, Jul. 2021.
[34] Z. Zhang *et al.*, "Dense residual network: Enhancing global dense feature flow for character recognition," *Neural Netw.*, vol. 139, pp. 77–85, Jul. 2021.
[35] A. A. Adegun and S. Viriri, "FCN-based DenseNet framework for automated detection and classification of skin lesions in dermoscopy images," *IEEE Access*, vol. 8, pp. 150377–150396, 2020.
[36] N. Aldoj, F. Biavati, F. Michallek, S. Stober, and M. Dewey, "Automatic prostate and prostate zones segmentation of magnetic resonance images using DenseNet-like U-net," *Sci. Rep.*, vol. 10, no. 1, p. 14315, Aug. 2020.
[37] S. Zhai, D. Shang, S. Wang, and S. Dong, "DF-SSD: An improved SSD object detection algorithm based on DenseNet and feature fusion," *IEEE Access*, vol. 8, pp. 24344–24357, 2020.
[38] Z. Mo, D. Luo, T. Wen, Y. Cheng, and X. Li, "FPGA implementation for odor identification with depthwise separable convolutional neural network," *Sensors*, vol. 21, no. 3, p. 832, Jan. 2021.
[39] J. C. Rodriguez Gamboa, A. J. da Silva, I. C. S. Araujo, E. S. Albarracin, and C. M. Duran A., "Validation of the rapid detection approach for enhancing the electronic nose systems performance, using different deep learning models and support vector machines," *Sens. Actuators B, Chem.*, vol. 327, Jan. 2021, Art. no. 128921.
[40] S. Zhang, Y. Cheng, D. Luo, J. He, A. K. Y. Wong, and K. Hung, "Channel attention convolutional neural network for Chinese baijiu detection with E-nose," *IEEE Sensors J.*, vol. 21, no. 14, pp. 16170–16182, Jul. 2021.
[41] X. Zhao, Z. Wen, X. Pan, W. Ye, and A. Bermak, "Mixture gases classification based on multi-label one-dimensional deep convolutional neural network," *IEEE Access*, vol. 7, pp. 12630–12637, 2019.
[42] Y. Wang *et al.*, "An optimized deep convolutional neural network for dendrobium classification based on electronic nose," *Sens. Actuators A, Phys.*, vol. 307, Jun. 2020, Art. no. 111874.
[43] T. Zhang, G. Qi, B. Xiao, and J. Wang, "Interleaved group convolutions for deep neural networks," in *Proc. IEEE Int. Conf. Comput. Vis.*, Jul. 2017, pp. 4383–4392.
[44] Y. Zhang, Y. Tian, Y. Kong, B. Zhong, and Y. Fu, "Residual dense network for image super-resolution," in *Proc. IEEE Conf. Comput. Vis. Pattern Recognit.*, Jun. 2018, pp. 2472–2481.

Yan Shi (Member, IEEE) was born in Jilin, China. He received the B.E. and M.E. degrees from the School of Automation Engineering, Northeast Electric Power University, Jilin, China, in 2015 and 2018, respectively. He is currently pursuing the Ph.D. degree in automation engineering with Northeast Electric Power University.

He has published 12 articles in the fields of electrical engineering, instrument science, pattern recognition, and quality inspection. His research interests include sensor fabrication, electronic nose, feature mining, quality inspection, and deep learning.

Hangcheng Yuan was born in Xinjiang, China. He received the B.E. degree from the School of Information Engineering, Southwest University of Science and Technology, Mianyang, Sichuan, China, in 2019. He is currently pursuing the M.E. degree in automation engineering with Northeast Electric Power University, Jilin, China.

His research interests include the design and development of electronic nose, sensor applications, deep learning, and feature mining.

Qinglun Zhang was born in Sichuan, China, in 2001. He is currently pursuing the B.S. degree in automation engineering with Northeast Electric Power University, Jilin, China.

His research interests include deep learning and pattern recognition in engineering applications.

Ao Sun was born in Jilin, China. He received the B.E. degree from the School of Electrical Engineering, Northeast Electric Power University, Jilin, in 2019. He is currently pursuing the M.E. degree in electrical engineering with Northeast Electric Power University.

His research interests include deep learning and pattern recognition, system optimization, and industrial monitoring.

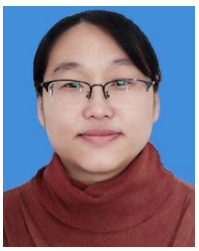

Jingjing Liu was born in Jilin, China. She received the Ph.D. degree from the School of Biology, Jilin University, Jilin, in 2013. She completed the post-doctoral research at the School of Biomedical Engineering and Instrument Science, Zhejiang University, Hangzhou, China, in 2019.

She is currently an Associate Professor with the School of Electrical Engineering, Northeast Electric Power University, Jilin. She has published more than 30 peer-reviewed articles. Her research interests include the electronic nose, industrial environment monitoring, and pattern recognition.

Hong Men was born in Jilin, China. He received the M.E. degree from the School of Electrical Engineering, Northeast Electric Power University, Jilin, in 2002, and the Ph.D. degree from the School of Biomedical Engineering and Instrument Science, Zhejiang University, Hangzhou, China, in 2005.

He is currently a Professor in automation engineering with Northeast Electric Power University, Jilin. He has authored or coauthored more than 50 peer-reviewed articles on his research interests, which include sensor fabrication, electronic nose, machine perception technology, and pattern recognition.

Dr. Men was a recipient of the Science and Technology Progress First Prize of Jilin Province, China, in 2012, and the Science and Technology Progress Second Prize of Jilin Province, China, in 2014 and 2016.